Temporal forcing of small-amplitude waves in anisotropic systems

Hermann Riecke*
Department of Engineering Sciences and Applied Mathematics, Northwestern University, Evanston, Illinois 60208

Mary Silber†
Department of Applied Mechanics, California Institute of Technology, Pasadena, California 91125

Lorenz Kramer*
Physikalisches Institut, Universität Bayreuth, D-95440 Bayreuth, Germany
(Received 17 September 1993)

We investigate the effect of resonant temporal forcing on an anisotropic system that exhibits a Hopf bifurcation to obliquely traveling waves in the absence of this forcing. We find that the forcing can excite various phase-locked standing-wave structures: rolls, rectangles, and cross rolls. At onset, at most one of the two—rolls or rectangles—is stable. The cross rolls can arise in a secondary bifurcation and can be stable. Experimentally, they would appear as a periodic switching between a structure in which the "zig" component dominates and one with a dominating "zag" structure. Since there are two symmetry-related states of this kind, one may expect disordered structures to arise due to the breakup of the pattern into domains. The results are consistent with recent experiments on electroconvection in nematic liquid crystals by de la Torre Juárez and Rehberg [Phys. Rev. A **42**, 2096 (1990)]. We also apply the general analysis to a model of the behavior near a Lifshitz point, where the angle of obliqueness vanishes. This analysis indicates that phase-locked standing rectangles are always unstable in this parameter regime.

PACS number(s): 47.20.Ky, 03.40.Kf, 47.27.Te

I. INTRODUCTION

Temporally periodic forcing can qualitatively change the behavior of systems exhibiting spatial or spatio-temporal structures. In systems which form oscillatory structures, strongly resonant temporal forcing has a particularly large impact. For example, in one-dimensional systems that undergo a Hopf bifurcation to stable traveling waves, forcing can excite stable standing waves below the threshold for the traveling waves; these standing waves are phase locked to the forcing [1–3]. This theoretical prediction has been confirmed experimentally in Taylor-Dean flow [4] and in electrohydrodynamic convection (EHC) of nematic liquid crystals [5].

In the nematic phase, the liquid-crystal system exhibits an axial anisotropy due to a partial alignment of the molecules; this defines the director. In the first EHC experiments the waves always propagated along the director [5]. Recently the experimental parameter regime has been extended to include a regime in which disordered patches of waves, traveling at an *oblique* angle to the director, are observed [6]. In this case, temporally periodic forcing excites standing waves in the form of either oblique rolls or rectangles. In addition, more complicated structures are found [6]. These observations provide the experimental motivation for our theoretical investigation.

This paper examines the effect of resonant forcing on oblique traveling waves produced in a Hopf bifurcation of the spatially uniform state of a two-dimensional anisotropic system. The symmetry of the system forces coexistence of waves traveling in four directions. The possible interactions of these waves make a complete analysis of the problem extremely complicated. However, one of the striking features of the excited roll and rectangular structures is their strong spatial coherence. This suggests that as a first step we focus on the case where the amplitudes of the different modes are space independent. We therefore investigate an extension of the four complex amplitude equations analyzed previously [8]; this model takes the temporal forcing into account [9], but neglects large-scale spatial variations in the amplitudes. This analysis elucidates the connection between the different structures excited in the experiments and allows us to make some predictions for future experiments. We also consider the transition from oblique to normal traveling waves using suitably extended coupled Ginzburg-Landau equations which are valid close to a Lifshitz point where the angle of obliqueness goes to zero.

Formally, our analysis applies to weakly forced waves arising through a Hopf bifurcation. We expect, however, that some aspects may pertain to parametrically excited waves in systems that do not undergo a Hopf bifurcation, but which support weakly damped waves in the absence of forcing. In particular, this approach has been suc-

*Also at Institute for Theoretical Physics, University of California, Santa Barbara, CA 93106.

†Present address: Department of Engineering Sciences and Applied Mathematics, Northwestern University, Evanston, IL 60208.

cessfully applied to surface waves arising in the Faraday experiment with low-viscosity liquids [10] and is related to methods used in studies of spin waves in ferromagnets [11]. Of course, when applying the present approach to these systems only the phenomena arising in the linearly damped regime are of relevance (i.e., for parameter values below the Hopf bifurcation point).

The organization of the paper is as follows. Section II presents the amplitude equations for weakly forced oblique waves. Section III reviews and interprets results on the transition from traveling waves to phase-locked standing waves. The phase-locked structures, as well as the transitions between them, are discussed in detail in Sec. IV. Section V contains our analysis of the Lifshitz equations. The theoretical results are then compared with the experimental ones in Sec. VI. The main results of the paper are summarized in the conclusion, Sec. VII.

II. AMPLITUDE EQUATIONS FOR RESONANTLY FORCED OBLIQUE WAVES

This paper focuses on Hopf bifurcation in axially anisotropic systems in the case where there are four neutrally stable modes at the Hopf bifurcation point. These modes correspond to waves that travel at an oblique angle γ to the axis of anisotropy. Thus a typical scalar field such as the vertical component of the velocity in convection, V_z, is given by

$$\begin{aligned} V_z(x,y,t) = (&z_1 e^{i(qx+py)} + z_2 e^{i(-qx+py)} \\ &+ z_3 e^{-i(qx+py)} + z_4 e^{-i(-qx+py)}) \\ &\times e^{i\omega_e t/n} + \text{c.c.} + \text{h.o.t.} \end{aligned} \tag{1}$$

Here we have suppressed any dependence of V_z on the vertical coordinate z; ω_e is the external forcing frequency, and h.o.t. denotes higher-order terms. Since we are considering resonant forcing of order n, we assume that ω_e/n is close to the Hopf frequency. In this paper, we treat the strong resonant cases $n = 1, 2$. For the EHC experiments of interest $n = 2$ [6]. Note that z_1 and z_3 correspond to left- and right-traveling plane waves in the direction of $q\hat{\mathbf{x}} + p\hat{\mathbf{y}}$; similarly z_2 and z_4 correspond to oppositely traveling plane waves in the direction of $-q\hat{\mathbf{x}} + p\hat{\mathbf{y}}$. Thus the waves travel at an oblique angle $\gamma = \tan^{-1}(p/q)$ to the x axis (the axis of anisotropy). Here we assume that the amplitudes z_i are complex-valued functions of a slow time T, but that they do not depend on the spatial coordinates. The time evolution of the amplitudes is determined by a system of coupled first order ordinary differential equations which can, in principle, be derived from the governing hydrodynamic equations (with periodic boundary conditions) using center-manifold reduction [12]. However, in EHC this is not yet possible; even the origin of the Hopf bifurcation has not been understood at the hydrodynamic level [13]. Nevertheless, the general form of the amplitude equations can be determined from symmetry considerations assuming that the waves are due to a Hopf bifurcation of the motionless state as experiments suggest [14]. Consequently, most of our results are not specific to the EHC experiments, but pertain to a larger class of resonantly forced systems with the same underlying symmetries. In a more heuristic fashion, we also expect our results to be relevant to surface waves in the Faraday experiment [15]. We will, however, focus on the EHC system in order to make contact with available experiments [6].

We consider a general system that is invariant under translations in the plane; since our solutions are spatially doubly periodic, the group of translations corresponds to a torus T^2. Moreover, we assume reflection symmetries in planes parallel and perpendicular to the axis of anisotropy; these reflections are denoted by κ_1 and κ_2, where $\kappa_1 : (x,y) \to (x,-y)$ and $\kappa_2 : (x,y) \to (-x,y)$. These spatial symmetries act on the amplitudes as follows:

$$(\theta_1,\theta_2) : \begin{pmatrix} z_1 \\ z_2 \\ z_3 \\ z_4 \end{pmatrix} \to \begin{pmatrix} e^{i\theta_1} z_1 \\ e^{i\theta_2} z_2 \\ e^{-i\theta_1} z_3 \\ e^{-i\theta_2} z_4 \end{pmatrix},$$

$$\kappa_1 : \begin{pmatrix} z_1 \\ z_2 \\ z_3 \\ z_4 \end{pmatrix} \to \begin{pmatrix} z_4 \\ z_3 \\ z_2 \\ z_1 \end{pmatrix}, \quad \kappa_2 : \begin{pmatrix} z_1 \\ z_2 \\ z_3 \\ z_4 \end{pmatrix} \to \begin{pmatrix} z_2 \\ z_1 \\ z_4 \\ z_3 \end{pmatrix}. \tag{2}$$

Here the phase shift θ_1 results from a translation $(x,y) \to (x+\theta_1/2q, y+\theta_1/2p)$ and the θ_2 phase shift results from a translation by $(-\theta_2/2q, \theta_2/2p)$. The amplitude equations are equivariant with respect to these transformations. In the absence of resonant temporal forcing the normal form of the amplitude equations possesses an additional phase-shift symmetry that we interpret as a time-translation symmetry $t \to t + \phi/\omega_h$. It acts on the amplitudes as follows:

$$\phi : \mathbf{z} \to e^{i\phi}\mathbf{z}, \tag{3}$$

where $\mathbf{z} \equiv (z_1, z_2, z_3, z_4)$. An analysis of the cubic truncation of the amplitude equations, equivariant with respect to the symmetries (2) and (3), is presented in [8].

The temporal forcing destroys the phase-shift symmetry (3), thereby allowing additional terms in the amplitude equations. We assume that the temporal forcing is weak and therefore we keep only the lowest order term which does not satisfy the time-translation symmetry (3). The amplitude equations truncated at cubic order are [9]

$$\begin{aligned} \dot{z}_1 &= \nu z_1 + \mu z_3^* + \left(a|z_1|^2 + b|z_2|^2 + c|z_3|^2 + d|z_4|^2\right) z_1 \\ &\quad + f\, z_2 z_3^* z_4, \\ \dot{z}_2 &= \nu z_2 + \mu z_4^* + \left(a|z_2|^2 + b|z_1|^2 + c|z_4|^2 + d|z_3|^2\right) z_2 \\ &\quad + f\, z_1 z_4^* z_3, \\ \dot{z}_3 &= \nu z_3 + \mu z_1^* + \left(a|z_3|^2 + b|z_4|^2 + c|z_1|^2 + d|z_2|^2\right) z_3 \\ &\quad + f\, z_2 z_1^* z_4, \\ \dot{z}_4 &= \nu z_4 + \mu z_2^* + \left(a|z_4|^2 + b|z_3|^2 + c|z_2|^2 + d|z_1|^2\right) z_4 \\ &\quad + f\, z_1 z_2^* z_3 \,. \end{aligned} \tag{4}$$

There are three small unfolding parameters: the distance from the Hopf bifurcation in the absence of forcing,

$\mathrm{Re}\{\nu\} \equiv \nu_r$, the detuning ν_i of the forcing frequency ω_e with respect to the linear frequency ω_0, $\nu_i \equiv \mathrm{Im}\{\nu\} = \omega_0 - \omega_e/n$ $(n = 1, 2)$, and the forcing amplitude F, $|\mu|^n \propto F^2$ [1,2]. (In the case of parametrically excited, weakly damped waves, ν_r is proportional to the linear damping of the waves; it is always negative.) Without loss of generality, we choose the temporal phase of the forcing such that μ is real and positive; all other coefficients are complex.

In the absence of forcing ($\mu = 0$) Eqs. (4) possess up to seven branches of periodic solutions that bifurcate from the origin at $\nu_r = 0$. Three of these correspond to different types of traveling waves and four to (superpositions) of standing waves. In particular, they have the form

$$\begin{array}{lll} \mathrm{I}: & \mathbf{z} = (v,0,0,0) & \mathrm{TRo}, \\ \mathrm{II}: & \mathbf{z} = (v,v,0,0) & \mathrm{TRe}^{\perp}, \\ \mathrm{III}: & \mathbf{z} = (v,0,0,v) & \mathrm{TRe}^{\parallel}, \\ \mathrm{IV}: & \mathbf{z} = (v,0,v,0) & \mathrm{SRo}, \\ \mathrm{V}: & \mathbf{z} = (v,v,v,v) & \mathrm{SRe}, \\ \mathrm{VI}: & \mathbf{z} = (v,iv,v,iv) & \mathrm{ARo}, \\ \mathrm{VII}: & \mathbf{z} = (v_1,v_2,v_1,v_2) & \mathrm{SCR}. \end{array} \tag{5}$$

The abbreviations denote traveling rolls (TRo), two kinds of traveling rectangles distinguished by their direction of propagation relative to the axis of anisotropy ($\mathrm{TRe}^{\perp}$,$\mathrm{TRe}^{\parallel}$), standing rolls (SRo), standing rectangles (SRe), alternating rolls (ARo), and standing cross rolls (SCR). The standing cross rolls, which are characterized by two complex amplitudes v_1 and v_2, do not always exist. The numbering is the same as that used in our previous work on the unforced system [8]. In addition to these periodic solutions one finds more complicated (branches of) attractors such as heteroclinic cycles connecting three of the above solutions [8].

In the presence of forcing, oppositely traveling waves are linearly coupled [see Eq. (4)] so that pure traveling waves do not exist. For example, the forcing destroys pure right-traveling $\mathrm{TRe}^{\parallel}$ by coupling it to the left-traveling $\mathrm{TRe}^{\parallel}$; thus the $\mathrm{TRe}^{\parallel}$ are replaced by a general superposition of left- and right-traveling rectangles, i.e., by (v_1, v_2, v_2, v_1). Similarly, forcing destroys the ARo solution, which is an equal-amplitude superposition of standing rolls which differ by $\pi/2$ in their temporal phase. In the next section we see that the pure standing waves (SRo and SRe) persist and that they can phase lock to the temporally periodic forcing.

III. TRAVELING VS PHASE-LOCKED STANDING WAVES

In this section we study the effects of resonant forcing on competition between various traveling-wave structures and their standing-wave counterparts. Specifically, we focus on the stability of the phase-locked standing waves to traveling-wave disturbances. In the oblique regime there are two simple types of phase-locked standing waves (PSW): phase-locked standing rolls (PSRo) and phase-locked standing rectangles (PSRe). The stability of the PSRo state to traveling disturbances is determined by restricting (4) to the subspace where $\mathbf{z} = (v_1, 0, v_2, 0)$. Similarly the stability of PSRe to traveling disturbances is determined by restricting (4), in turn, to each of the subspaces where $\mathbf{z} = (v_1, v_1, v_2, v_2)$ and $\mathbf{z} = (v_1, v_2, v_2, v_1)$; in the former case the disturbances travel perpendicular to the director, whereas in the latter case they travel along it. In each of these three cases, the restricted dynamics has the form

$$\begin{aligned} \dot{v}_1 &= \nu v_1 + \mu v_2^* + \alpha v_1 |v_1|^2 + \beta v_1 |v_2|^2, \\ \dot{v}_2 &= \nu v_2 + \mu v_1^* + \beta v_2 |v_1|^2 + \alpha v_2 |v_2|^2, \end{aligned} \tag{6}$$

where

$$\alpha = a, \quad \beta = c \quad \text{for TRo}, \tag{7a}$$

$$\alpha = a + b, \quad \beta = c + d + f \quad \text{for } \mathrm{TRe}^{\perp}, \tag{7b}$$

$$\alpha = a + d, \quad \beta = b + c + f \quad \text{for } \mathrm{TRe}^{\parallel}. \tag{7c}$$

Here the subspaces are denoted by the traveling waves that are present in each of them when there is no resonant forcing [cf. (5)]. Equation (6) was studied previously in the context of periodically forced waves in one dimension [1–3]; in these papers the phase-locked standing waves, as well as traveling (TW) and unlocked standing waves (SW), were investigated. The results apply directly to the present system by an appropriate identification of TRo and $\mathrm{TRe}^{\parallel,\perp}$ with the traveling wave TW, and the new phase-locked solutions PSRo and PSRe with the standing wave PSW.

In Fig. 1 we sketch a typical phase diagram associated with (6), for fixed detuning ν_i and for $\beta_r < \alpha_r < 0$; in this case the unforced traveling waves bifurcate supercritically and are stable. In the following discussion we employ the notation (TW, PSW) used in the one-dimensional case. For weak forcing the trivial equilibrium loses stability via Hopf bifurcation along the line marked H; this bifurcation leads to stable traveling waves, TW, for positive values of ν_r. (The unlocked standing waves,

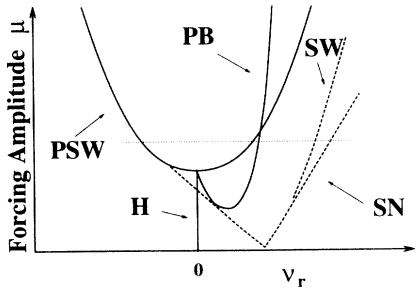

FIG. 1. Phase diagram for a periodically forced supercritical Hopf bifurcation to traveling waves in the (ν_r, μ) plane, where ν_r is the distance from the Hopf bifurcation in the absence of forcing and μ is the forcing amplitude. Phase-locked standing waves bifurcate from the motionless state on the line PSW, traveling waves bifurcate at the line marked H. The standing waves undergo a parity-breaking bifurcation at PB, a saddle-node bifurcation at SN, and a Hopf bifurcation to unlocked standing waves at SW.

SW, are unstable in this case.) Along the line marked PSW, which is given by $\mu^2 = |\nu|^2$, a steady bifurcation of the zero solution of (6) occurs; this bifurcation produces the phase-locked standing waves PSW with frequency ω_e/n. The amplitude $r = |v_1| = |v_2|$ of the PSW satisfies

$$|N|^2 r^4 + 2r^2 \mathrm{Re}\{\nu^* N\} + |\nu|^2 - \mu^2 = 0, \tag{8}$$

where $N \equiv \alpha + \beta$. If $\mathrm{Re}\{\nu^* N\} \equiv \nu_r N_r + \nu_i N_i > 0$ the bifurcation to PSW is forward, otherwise backward. Thus, depending on the detuning ν_i, the bifurcation to the PSW can be in either direction, independent of the bifurcation direction of the standing waves in the unforced Hopf bifurcation. The saddle-node line of the PSW, marked SN in Fig. 1, is given by

$$\mu^2 = (\mathrm{Im}\{\nu^* N\})^2 / |N|^2, \tag{9}$$

for $\mathrm{Re}\{\nu^* N\} < 0$.

The linear stability analysis of the PSW is simplified by the fact that the perturbations (u_1, u_2) of the steady solution $(v_1, v_2) = (v, v)$ of (6) fall into two classes: $u_1 = u_2$ and $u_1 = -u_2$. We focus first on the perturbations that preserve the standing-wave character of the waves $(u_1 = u_2)$. The determinant and trace of the resulting 2×2 stability matrix are

$$\det = |\nu + 2Nr^2|^2 - |\nu|^2, \tag{10}$$

$$\mathrm{Tr} = 2(\nu_r + 2N_r r^2), \tag{11}$$

where r^2 solves (8). The determinant vanishes at the saddle-node bifurcation (9). There is a secondary Hopf bifurcation when the trace vanishes, provided the determinant is positive. This bifurcation produces unlocked standing waves SW. The perturbations of the form $u_1 = -u_2$ include the marginal translation mode and a parity-breaking instability to traveling waves. The parity-breaking instability occurs when the trace of the associated Jacobian matrix vanishes, i.e., when

$$\mathrm{Tr} = 2(\nu_r + 2\alpha_r r^2) = 0. \tag{12}$$

It is denoted by PB in Fig. 1. A typical bifurcation diagram is presented in Fig. 2. As long as the unforced traveling waves are stable with respect to the standing waves ($\beta_r < 0$), the secondary Hopf bifurcation of the PSW to unlocked standing waves is always preempted by the parity-breaking bifurcation to traveling waves. In addition, modulated waves exhibiting three different frequencies are possible; this follows from an analysis of Eq. (6) in the vicinity of the point where the Hopf bifurcation and the steady bifurcation merge ($\mu^2 = \nu_i^2, \nu_r = 0$) [1]. This codimension-two point corresponds to a Takens-Bogdanov bifurcation with O(2) symmetry, which was analyzed by Dangelmayr and Knobloch [16].

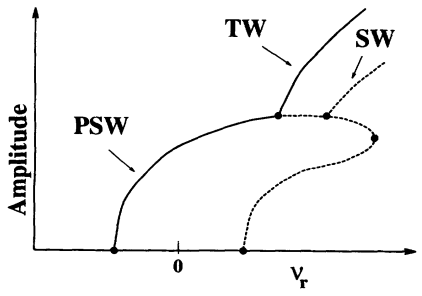

FIG. 2. Typical bifurcation diagram for a periodically forced supercritical Hopf bifurcation to traveling waves as obtained along the dotted line in Fig. 1.

Thus the stability of the phase-locked states (PSRo, PSRe) to traveling disturbances (TRo, $\mathrm{TRe}^{\perp,\parallel}$) and to unlocked standing waves (SRo, SRe) is understood in some detail based on previous studies. The competition between the different kinds of phase-locked standing waves is the subject of the next section.

IV. COMPETITION BETWEEN PHASE-LOCKED STANDING ROLLS AND STANDING RECTANGLES

The relative stability of PSRo and PSRe is particularly relevant to our understanding of the EHC experiments since both states are observed. This stability question can be addressed by restricting (4) to the standing-cross-rolls subspace where $(z_1, z_2, z_3, z_4) = (v_1, v_2, v_1, v_2)$. Note that this subspace contains both the PSRo ($v_1 = 0$ or $v_2 = 0$) and the PSRe ($v_1 = v_2$) solutions. The amplitudes v_1 and v_2 satisfy

$$\begin{aligned} \dot{v}_1 &= \nu v_1 + \mu v_1^* + (a+c) v_1 |v_1|^2 + (b+d) v_1 |v_2|^2 + f v_1^* v_2^2, \\ \dot{v}_2 &= \nu v_2 + \mu v_2^* + (b+d) v_2 |v_1|^2 + (a+c) v_2 |v_2|^2 + f v_2^* v_1^2. \end{aligned} \tag{13}$$

These equations differ from those describing the forced O(2)-Hopf bifurcation (6); the modes with amplitudes v_1 and v_2 are uncoupled at the linear level since they represent standing waves with different orientations. Moreover, the nonlinear coupling term with coefficient f is absent in (6).

We focus first on the stability of the PSRo solution, which has the form $(v_1, v_2) = (u, 0)$, to perturbations in the $(0, v_2)$ direction. The resulting 2×2 stability matrix D_{PSRo} has the following trace and determinant:

$$\mathrm{Tr}(D_{\mathrm{PSRo}}) = 2[\nu_r + (b_r + d_r) r_{\mathrm{PSRo}}^2], \tag{14}$$

$$\det(D_{\mathrm{PSRo}}) = |\nu + (b+d) r_{\mathrm{PSRo}}^2|^2 - |\nu + (a+c-f) r_{\mathrm{PSRo}}^2|^2. \tag{15}$$

The amplitude r_{PSRo} satisfies (8) with $N = a + c$. Provided the determinant (15) is positive, there is a Hopf bifurcation at $\nu_r = -(b_r + d_r) r_{\mathrm{PSRo}}^2$; thus the presence of the PSRo in one direction leads to a shift of the primary Hopf bifurcation in the other direction. A steady state bifurcation occurs for

$$\frac{r_{\mathrm{PSRo}}^2}{2} = \rho \equiv \frac{\mathrm{Re}\{\nu^*(a+c-b-d-f)\}}{|b+d|^2 - |a+c-f|^2}. \tag{16}$$

We will show that this bifurcation leads to phase-locked standing cross rolls PSCR which are also pertinent to the

EHC experiments. The PSRo are stable in the $(0, v_2)$ direction as long as the trace (14) is negative and

$$2\,\mathrm{Re}\,\{\nu^*(a+c-b-d-f)\}$$

$$< \left(|b+d|^2 - |a+c-f|^2\right) r_{\mathrm{PSRo}}^2. \quad (17)$$

Note that ρ depends on both the control parameters ν_r and ν_i. Moreover, since the amplitude r_{PSRo} can be varied independently of ν by changing the forcing amplitude μ, Eq. (17) reduces at onset to

$$2\,\mathrm{Re}\,\{\nu^*(a+c-b-d-f)\} < 0. \quad (18)$$

Finally we note that the symmetry of the PSRo solution results in a doubling of the eigenvalues associated with perturbations at an oblique angle to the rolls (see, for example, [7]). Hence the stability calculations of this section actually determine four of the eight eigenvalues of the full stability matrix associated with (4) linearized about PSRo; the remaining four eigenvalues were determined in the preceding section.

We now examine the stability of the phase-locked standing rectangles in the standing-cross-rolls subspace. The PSRe solution is an equilibrium solution of (13) of the form $(v_1, v_2) = (u, u)$. We examine its stability with respect to perturbations of the form $(w, -w)$ by substituting $(v_1, v_2) = (u+w, u-w)$ in (13). The resulting 2×2 stability matrix D_{PSRe} has the following trace and determinant:

$$\mathrm{Tr}(D_{\mathrm{PSRe}}) = 2\nu_r + 4(a_r + c_r - f_r) r_{\mathrm{PSRe}}^2, \quad (19)$$

$$\det(D_{\mathrm{PSRe}}) = |\nu + 2(a+c-f) r_{\mathrm{PSRe}}^2|^2 - |\nu + 2(b+d) r_{\mathrm{PSRe}}^2|^2, \quad (20)$$

where r_{PSRe} is a solution of (8) with $N = a+b+c+d+f$. Note that

$$\det[D_{\mathrm{PSRo}}(r_{\mathrm{PSRo}}^2)] = -\det[D_{\mathrm{PSRe}}(2r_{\mathrm{PSRe}}^2)]. \quad (21)$$

Consequently a steady bifurcation to PSCR occurs at

$$r_{\mathrm{PSRe}}^2 = \rho, \quad (22)$$

where ρ is defined in (16). The coincidence of the steady state bifurcations of the PSRe and the PSRo branches, both to PSCR solutions, suggests that they may be connected by the *same* branch of PSCR; this provides a mechanism for a continuous transition between PSRo and PSRe. We will show, in a particular limit, that this possibility can occur.

The PSCR are steady state solutions of (13) with $v_1 v_2 \neq 0$ and $|v_1| \neq |v_2|$. We let $v_1 = \mathrm{Re}^{i\Phi}$ and $v_2 = re^{i\phi}$, and eliminate the phases from (13) to obtain (for $r \neq 0$)

$$\mu^2 = \left| \nu + (a+c) r^2 + (b+d) R^2 + f R^2 \frac{\nu + (a+c-f) r^2 + (b+d) R^2}{\nu + (b+d) r^2 + (a+c-f) R^2} \right|^2. \quad (23)$$

Moreover, if r and R are both nonzero, then

$$|\nu + (b+d)R^2 + (a+c-f)r^2|^2 = |\nu + (a+c-f)R^2 + (b+d)r^2|^2. \quad (24)$$

This has a solution $r^2 = R^2$, which corresponds to the PSRe, and also a solution

$$r^2 + R^2 = 2\rho. \quad (25)$$

Substituting $r^2 = 2\rho - R^2$ in (23) leads to a quartic equation for R^2:

$$C_8 R^8 + C_6 R^6 + C_4 R^4 + C_2 R^2 + C_0 = 0. \quad (26)$$

The coefficients C_0, C_2, and C_8 are given by

$$C_0 = |\nu + 2(b+d)\rho|^2 [|\nu + 2(a+c)\rho|^2 - \mu^2], \quad (27)$$

$$C_2 = 2\,\mathrm{Re}([\nu + 2(b+d)\rho]\,(h^* - f^*) \times \{2\rho[\nu + 2(a+c)\rho](h^* + f^*) - \mu^2\}), \quad (28)$$

$$C_8 = |h^2 - f^2|^2, \quad (29)$$

where $h \equiv a+c-b-d$. We use the reflection symmetry that interchanges $R^2 = |v_1|^2$ and $r^2 = |v_2|^2$ to simplify this equation. In particular, we observe that for each solution R_1^2 there must also exist a solution $R_2^2 = 2\rho - R_1^2$ [cf. (25)]. We let

$$u \equiv R^2(2\rho - R^2) \quad (30)$$

and write the solutions to (26) as

$$u = \frac{-C_2 \pm \sqrt{C_2^2 - 16 C_0 C_8 \rho^2}}{4\rho C_8}, \quad (31)$$

which yields the symmetry-related pair of solutions

$$R^2 = \rho \pm \sqrt{\rho^2 - u}. \quad (32)$$

Note that both u and R^2 must be positive for PSCR to exist. From (31), it follows that there are at most *two* distinct PSCR solutions of (13); these annihilate in a saddle-node bifurcation when $C_2^2 = 16 C_0 C_8 \rho^2$. We note that the PSCR solution merges with the PSRo when $u = 0$ and with PSRe when $u = \rho^2$. We now consider two limiting cases in which we can show explicitly that the PSCR arise as a secondary solution branch that connects the PSRo and PSRe solutions.

The phase-locked standing waves arise through a steady bifurcation at $|\nu|^2 = \mu^2$, whenever $\nu_r < 0$, i.e., for values of ν_r below the unforced Hopf bifurcation point. We can use center manifold reduction [12] to reduce the complex equations (13) to two real equations for the standing-wave amplitudes [17]. For $|\nu|^2 = \mu^2$, $\nu_r < 0$, the neutral eigenspace of (13) linearized about the origin is spanned by $v_j = \eta_1 \equiv i(\mu + \nu^*)$, $j = 1, 2$; the damped eigendirections associated with the double eigenvalue $2\nu_r$ are given by $v_j = \eta_2 \equiv i(\mu - \nu)$. We introduce the slow time $\tau = \epsilon^2 T$ and let $v_j = \epsilon \eta_1 A_j + \epsilon^3(\eta_1 A_{j3} + \eta_2 B_{j3}) + \mathrm{h.o.t}$, $\mu = |\nu| + \epsilon^2 \mu_2$. At cubic order in ϵ we obtain

$$\frac{dA_1}{d\tau} = \sigma A_1 + \tilde{\alpha} A_1^3 + \tilde{\beta} A_1 A_2^2,$$
$$\frac{dA_2}{d\tau} = \sigma A_2 + \tilde{\alpha} A_2^3 + \tilde{\beta} A_2 A_1^2, \tag{33}$$

where

$$\sigma = -\frac{|\nu|\mu_2}{\nu_r}, \quad \tilde{\alpha} = \frac{|\eta_1|^2}{\nu_r}\mathrm{Re}\{\nu^*(a+c)\},$$
$$\tilde{\beta} = \frac{|\eta_1|^2}{\nu_r}\mathrm{Re}\{\nu^*(b+d+f)\}. \tag{34}$$

Equations of the form (33) also apply to systems with large damping whenever sufficiently large forcing is applied. In particular, these equations describe the oblique standing-wave components that have the correct temporal phase, relative to the periodic driver, to be excited by the forcing. In contrast, Eqs. (4) become invalid for large damping. Note that in general the amplitudes in (33) are complex due to translation symmetry; the specific choice for the standing-cross-rolls subspace ($z_1 \equiv z_3, z_2 \equiv z_4$) that leads to Eq. (13) breaks that symmetry.

Equations of the same form as (33) arise in the analysis of the O(2) Hopf bifurcation problem and have been studied extensively [18]. Generically, the only steady solutions of (33) have either equal amplitudes ($A_1 = A_2$), or one of the amplitudes vanishes. Thus at onset one has only PSRo (one vanishing amplitude) and PSRe ($A_1 = A_2$). Only in special degenerate cases do we expect more complicated small-amplitude equilibrium solutions near onset. In particular, if $\tilde{\alpha} \approx \tilde{\beta}$, then higher order terms must be included in the normal form (33) and there can exist a small-amplitude mixed-mode equilibrium solution with two different nonvanishing amplitudes [19,20]. The mixed-mode solution corresponds to the PSCR. Note that $\rho \propto (\tilde{\alpha} - \tilde{\beta})$ so that ρ is small in this degenerate situation. This is consistent with (16) and (22) which show that the secondary bifurcations to PSCR occur when the amplitudes r^2_{PSRo} and r^2_{PSRe} are of order ρ, respectively. In the two-dimensional control parameter space $(\mu_2, \tilde{\alpha} - \tilde{\beta})$ the regime in which the PSCR exist is delimited by the lines at which the PSRo and PSRe become unstable to PSCR. The stability of the PSCR solution depends on higher order terms which were neglected in deriving the amplitude equations (4) [19,20].

The center manifold equations (33) lose their validity when $\nu_r \to 0$ since the eigendirections with eigenvalue $2\nu_r$ can no longer be eliminated adiabatically; these standing-wave modes become independent dynamical variables. For nonzero detuning ν_i this regime can be analyzed by considering the Takens-Bogdanov double-zero point ($\nu_r = 0, \mu = \mu_0 \equiv |\nu_i|$) at which the Hopf frequency goes to zero. Near this point simplification is not achieved by a reduction in the number of degrees of freedom. Instead, the form of the linear operator allows certain nonlinear terms to be removed [12,21]. We begin by expanding the amplitudes along the two directions $\zeta_1 = (s+i)\mu_0$ and $\zeta_2 = 1$ in the complex plane, where $s \equiv \mathrm{sgn}(\nu_i)$ distinguishes between the cases of positive and negative detuning. Let

$$v_j = n(\zeta_1 \hat{A}_j + \zeta_2 \hat{B}_j), \quad j = 1,2, \quad 0 < n \ll 1. \tag{35}$$

The new dynamical variables $\hat{A}_j$ and $\hat{B}_j$ are real. At the double-zero point the linear part of (13) is

$$\dot{\hat{A}}_j = s\hat{B}_j, \tag{36a}$$
$$\dot{\hat{B}}_j = 0. \tag{36b}$$

Since $s \neq 0$, we can perform a near-identity nonlinear coordinate transformation that removes most of the cubic terms in the normal form. In particular, we let

$$A_1 = \hat{A}_1 + n^2(c_1\hat{A}_1^2 + c_2\hat{B}_1\hat{A}_1 + c_3\hat{A}_2^2 + c_4\hat{B}_2\hat{A}_2 + c_5\hat{B}_2^2)\hat{A}_1 + n^2(c_6\hat{B}_1^2 + c_7\hat{B}_1\hat{A}_1 + c_8\hat{A}_2^2 + c_9\hat{B}_2\hat{A}_2 + c_{10}\hat{B}_2^2)\hat{B}_1, \tag{37a}$$

$$B_1 = \hat{B}_1 + n^2(d_1\hat{A}_1^2 + d_2\hat{B}_1\hat{A}_1 + d_3\hat{A}_2^2 + d_4\hat{B}_2\hat{A}_2 + d_5\hat{B}_2^2)\hat{A}_1 + n^2(d_6\hat{B}_1^2 + d_7\hat{B}_1\hat{A}_1 + d_8\hat{A}_2^2 + d_9\hat{B}_2\hat{A}_2 + d_{10}\hat{B}_2^2)\hat{B}_1, \tag{37b}$$

with A_2 and B_2 defined by interchanging the 1 and 2 subscripts in (37a) and (37b), respectively. We choose the coefficients c_j and d_j so as to remove the cubic terms in the $\dot{\hat{A}}_j$ equations and four of the ten cubic terms in the $\dot{\hat{B}}_j$ equations. Moreover, in order to express the unfolding parameters of the resulting equations in terms of the original control parameters, we expand ν and μ as

$$\mu = \mu_0 + \epsilon\mu_1, \quad \nu = is\mu_0 + \epsilon(\nu_{r1} + i\nu_{i1}), \tag{38}$$

where $0 < \epsilon \ll 1$. The transformed equations are

$$\dot{A}_1 = sB_1 + \epsilon(\nu_{r1} + s\nu_{i1} - \mu_1)A_1 + \epsilon\nu_{i1}B_1/\mu_0 + \mathcal{O}(\epsilon n^2, n^4), \tag{39a}$$

$$\dot{B}_1 = \epsilon(\nu_{r1} - s\nu_{i1} + \mu_1)B_1 - 2\epsilon\mu_0(\nu_{i1} - s\mu_1)A_1$$
$$+4n^2\{-\mu_0^3(a_i + c_i)A_1^3 + 2\mu_0^2(a_r + c_r)B_1A_1^2 - \mu_0^3(b_i + d_i + f_i)A_1A_2^2$$
$$+\mu_0^2(b_r + d_r + 2f_r)B_2A_1A_2 + \mu_0^2(b_r + d_r)B_1A_2^2 + \mu_0(b_i + d_i - 2f_i)B_2B_1A_2\} + \mathcal{O}(\epsilon n^2, n^4), \tag{39b}$$

with similar equations for A_2 and B_2. We focus on the stationary solutions of (39a), (39b), which correspond to the phase-locked standing waves observed in the experiments. In this case, (39a) yields $B_j = \mathcal{O}(\epsilon, n^4)$, $j = 1, 2$, which takes all terms involving B_j in (39b) to higher order. We obtain the following algebraic equations for the A_j:

$$\begin{aligned} 0 = &-2\mu_0\{\epsilon(\nu_{i1} - s\mu_1) \\ &+2n^2\mu_0^2[(a_i + c_i)A_1^2 + (b_i + d_i + f_i)A_2^2]\}A_1 \\ &+\mathcal{O}(\epsilon^2, \epsilon n^2, n^4), \end{aligned} \tag{40}$$

$$\begin{aligned} 0 = &-2\mu_0\{\epsilon(\nu_{i1} - s\mu_1) \\ &+2n^2\mu_0^2[(a_i + c_i)A_2^2 + (b_i + d_i + f_i)A_1^2]\}A_2 \\ &+\mathcal{O}(\epsilon^2, \epsilon n^2, n^4). \end{aligned}$$

Note that the equations for the equilibrium solutions of (33) are of the same form as (40). Thus, as before, PSRo and PSRe are the only phase-locked standing waves in the vicinity of the Takens-Bogdanov point, unless $a_i + c_i \approx b_i + d_i + f_i$, in which case higher order terms must be retained. In this case, it is known that the existence region of PSCR lies between steady state instability lines of PSRo and PSRe [20]. Again this degenerate case corresponds to $\rho \approx 0$. (Recall that $\nu_r \approx 0$ near the Takens-Bogdanov point.)

We can combine the above results to obtain the following picture. The steady state instability at $\mu = |\nu|$ produces both PSRo and PSRe, with at most one of the two states being stable. This follows from (21); a positive determinant is necessary for stability and for $r^2_{\mathrm{PSRo,PSRe}} \to 0$ the determinants of D_{PSRo} and D_{PSRe} have opposite signs. (Recall that r^2 can be decreased by varying the control parameter μ, while holding ν fixed.) In addition, for ν_r sufficiently negative, i.e., below the onset of unforced traveling waves, the traces of D_{PSRo} (14) and D_{PSRe} (19) are both negative. For ρ sufficiently small, the steady bifurcations from PSRo and PSRe to PSCR can occur before the Hopf bifurcations associated with $\mathrm{Tr}(D_{\mathrm{PSRo}}) = 0$ and $\mathrm{Tr}(D_{\mathrm{PSRe}}) = 0$. The difference in the steady state bifurcation values for each of the solutions is given by

$$\begin{aligned} \Delta\mu^2 &\equiv \mu^2_{\mathrm{PSRo}\to\mathrm{PSCR}} - \mu^2_{\mathrm{PSRe}\to\mathrm{PSCR}} \\ &= \rho^2[2(|b + d|^2 - |a + c - f|^2) \\ &\quad -(|a + c + b + d + f|^2 - 4|a + c|^2)]. \end{aligned} \tag{41}$$

The two bifurcations coincide for $\rho = 0$ in which case they lie on the neutral curve $\mu^2 = |\nu|^2$. For $\rho < 0$ there is no bifurcation to PSCR. For $\rho > 0$ there are two main cases distinguished by the sign of $|b + d|^2 - |a + c - f|^2$ [cf. (17)]. In these two cases, the conditions for stability of PSRo and PSRe, respectively, to PSCR are given by

I $(|b + d|^2 - |a + c - f|^2 > 0)$:

$$\mathrm{PSRo}: \ r^2_{\mathrm{PSRo}} > 2\rho, \quad \mathrm{PSRe}: \ r^2_{\mathrm{PSRe}} < \rho, \tag{42a}$$

II $(|b + d|^2 - |a + c - f|^2 < 0)$:

$$\mathrm{PSRo}: \ r^2_{\mathrm{PSRo}} < 2\rho, \quad \mathrm{PSRe}: \ r^2_{\mathrm{PSRe}} > \rho. \tag{42b}$$

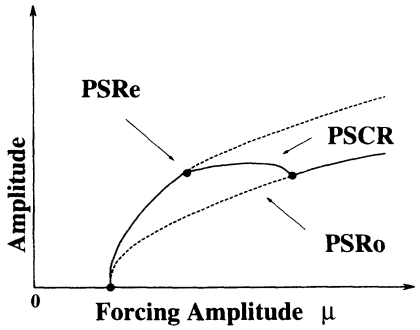

FIG. 3. Sketch of the bifurcation diagram of PSRo, PSRe, and PSCR for $\Delta\mu > 0$ and $\rho > 0$ in case I.

Figures 3 and 4 present possible bifurcation diagrams when $\rho > 0$, and when both PSRo and PSRe bifurcate supercritically. In case I, the PSRe are stable at onset, but become unstable to PSCR at larger amplitude (i.e., larger values of μ^2). For $\Delta\mu^2 > 0$, the PSCR merge with the PSRo for even larger μ^2 and stabilize them in turn. Our analysis does not determine whether the pitchfork bifurcation to the PSCR is supercritical or subcritical. In the simplest scenario, the bifurcation is supercritical when $\Delta\mu^2 > 0$ and the PSCR solution is stable in the SCR subspace. For $\Delta\mu^2 < 0$, the transition from PSRe to PSRo is hysteretic and (in the simplest case) the PSCR are unstable. In case II the PSRo and PSRe interchange their roles and stable PSCR are expected for $\Delta\mu^2 < 0$. If the PSRo or PSRe bifurcate subcritically from the basic state more complicated bifurcation diagrams are possible.

We emphasize that ρ depends on the control parameter ν. Within the present framework, one therefore expects that it may be possible to choose the detuning ν_i such that ρ is in a suitable range to observe the transition to PSCR below the onset of unforced waves ($\nu_r < 0$) and before other instabilities (e.g., parity breaking) set in. In particular, by choosing ν_i such that ρ is small and positive it may be possible to observe the transition between PSRo and PSRe by increasing μ. Whether this transition is made via a stable or unstable branch of PSCR solutions will depend on the nonlinear coefficients [see (41)]. Similarly, if both PSRo and PSRe bifurcate supercritically and ν_r is sufficiently negative, then ρ determines

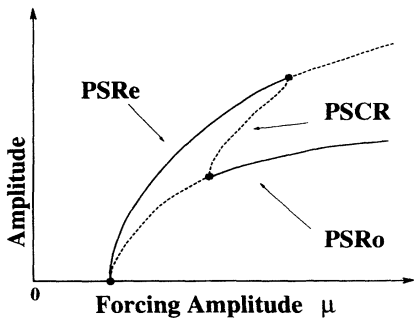

FIG. 4. Sketch of the bifurcation diagram of PSRo, PSRe, and PSCR for $\Delta\mu < 0$ and $\rho > 0$ in case I.

whether PSRo or PSRe are stable at onset. In particular, PSRo arise stably at onset if $\rho < 0$ in case I and if $\rho > 0$ in case II [see (16) and (18)]. As will be discussed below, the range over which the detuning and therefore ρ can be varied effectively is, however, limited in spatially extended systems.

V. TEMPORAL FORCING IN THE VICINITY OF A LIFSHITZ POINT

Experiments on the liquid-crystal system have identified a parameter regime where rolls travel along the axis of anisotropy as well as a parameter regime where (disordered) waves travel at an oblique angle to it. This is reminiscent of the situation of *steady* normal and oblique rolls for which the transition between the two regimes is usually continuous and the angle of obliqueness, $\gamma = \tan^{-1}(p/q)$ [cf. (1)], goes to zero at the Lifshitz point in parameter space [23,24]. In the present case of Hopf bifurcation to traveling rolls, the disordered character of the unforced waves has made experimental confirmation of the existence of such a Lifshitz point problematic; no such experimental verification exists to date. Nevertheless, such a point is of special interest since it provides a natural mechanism for a transition between the normal and oblique regimes. At the Lifshitz point, the critical modes with amplitudes z_1 and z_4 in (1) become indistinguishable as $\pm p \to 0$, as do the critical modes with amplitudes z_2, z_3; the description in terms of four ordinary differential equations is no longer appropriate. Instead, the behavior in the vicinity of the Lifshitz point is modeled by a generalized Ginzburg-Landau equation in which the small wave number p is incorporated into a slow variable in the y direction. This description of the Hopf bifurcation in the vicinity of the Lifshitz point is analogous to the model of the Lifshitz point in the steady state case [25]. The latter leads to a single partial differential equation (in two space dimensions) with real coefficients, whereas in the Hopf case the system is described by two coupled complex partial differential equations.

For a Hopf bifurcation with translation and reflection symmetry two complex amplitudes are required to model the behavior of both the left- and right-traveling waves. We replace (1) by

$$V_z(x,y,t) = \epsilon^2 A(x,y,t) e^{i(\omega_c \bar{t}/n + \bar{q}\bar{x})} + \epsilon^2 B(x,y,t) e^{i(\omega_c \bar{t}/n - \bar{q}\bar{x})} + \text{h.o.t.} + \text{c.c.}, \tag{43}$$

$0 < \epsilon \ll 1$, where $x = \epsilon^2 \bar{x}$, $y = \epsilon \bar{y}$, and $t = \epsilon^4 \bar{t}$ are slow variables. The spatial symmetries of the system result in the following equivariance properties of the generalized complex Ginzburg-Landau equations:

$$\bar{x} \to \bar{x} + \theta/\bar{q}: \quad (A, B, \partial_x, \partial_y) \to (Ae^{i\theta}, Be^{-i\theta}, \partial_x, \partial_y), \tag{44a}$$

$$\bar{x} \to -\bar{x}: (A, B, \partial_x, \partial_y) \to (B, A, -\partial_x, \partial_y), \tag{44b}$$

$$\bar{y} \to -\bar{y}: (A, B, \partial_x, \partial_y) \to (A, B, \partial_x, -\partial_y). \tag{44c}$$

One then obtains the following equations (through order ϵ^6):

$$\partial_t A - v\partial_x A = d\partial_x^2 A + s\partial_y^2 A + g\partial_x \partial_y^2 A + h\partial_y^4 A + \nu A + \mu B^* + \tilde{c}A(|A|^2 + |B|^2) + \tilde{g}A|B|^2,$$
$$\partial_t B + v\partial_x B = d\partial_x^2 B + s\partial_y^2 B - g\partial_x \partial_y^2 B + h\partial_y^4 B + \nu B + \mu A^* + \tilde{c}B(|A|^2 + |B|^2) + \tilde{g}B|A|^2, \tag{45}$$

where, without loss of generality, we assume that the group velocity v and the (scaled) forcing amplitude μ are real; all other coefficients are complex. The Lifshitz equations (46) without the temporal forcing (i.e., $\mu = 0$) were introduced in [9] and partially analyzed in [8]. In the unforced case the Lifshitz point is given by $s_r = \nu_r = 0$, with the unscaled deviation from the Lifshitz point given by $(\epsilon^2 s_r, \epsilon^4 \nu_r)$. As before we assume the temporal driving is small and therefore keep only the lowest order terms μB^* and μA^* that destroy the phase-shift symmetry $(A, B) \to e^{i\phi}(A, B)$. Specifically, the unscaled forcing is $\bar{\mu} = \epsilon^4 \mu$. Similarly, the complex coefficient ν has been scaled by ϵ^4, i.e., $\bar{\nu} = \epsilon^4 \nu$. It should be emphasized that all terms in (46) are not generally $\mathcal{O}(1)$ in ϵ. In particular, if the (unscaled) group velocity ($\bar{v}$) and the unscaled imaginary part of the s ($\bar{s}_i$) are $\mathcal{O}(1)$, then v and s_i are $\mathcal{O}(1/\epsilon^2)$. Formally, we assume that $\bar{v}$ and $\bar{s}_i$ are $\mathcal{O}(\epsilon^2)$ so that $\bar{v} = \epsilon^2 v$, $\bar{s} = \epsilon^2 s$. In an asymptotic analysis of the general case, where $\bar{v}$ and $\bar{s}_i$ are $\mathcal{O}(1)$, one would introduce a faster time $t_1 = \epsilon^2 \bar{t}$ and first solve the $\mathcal{O}(\epsilon^4)$ equations before introducing those at $\mathcal{O}(\epsilon^6)$ [26,27]. We expect to capture part of this general case by assuming v and s_i are large [i.e., $\mathcal{O}(1/\epsilon^2)$] in the final results.

Without temporal forcing, the growth rate σ of modes $A, B \propto e^{\pm i(qx+py)}$ is given by $\sigma = \nu_r - d_r q^2 - s_r p^2 + g_i q p^2 + h_r p^4$. Thus, for $s_r \geq 0$, a Hopf bifurcation to normal traveling rolls occurs at

$$\nu_r = 0, \; q_c = 0, \; p_c = 0. \tag{46}$$

For $s_r < 0$ the bifurcation to oblique traveling waves is given by

$$\nu_r = \frac{1}{2} s_r p_c^2, \; q_c = \frac{g_i s_r}{4h_r d_r + g_i^2}, \; p_c^2 = \frac{2d_r s_r}{4h_r d_r + g_i^2} > 0. \tag{47}$$

Note that stability of the trivial state with respect to large wave numbers q and p requires that $d_r > 0, h_r < 0$. Moreover, we assume $4h_r d_r + g_i^2 < 0$ so that the instability to oblique waves occurs when $s_r < 0$, with $\nu_r < 0$ in (47).

With resonant temporal forcing, the location of the Hopf bifurcation to normal, as well as to oblique, waves remains unchanged for small μ, i.e., for $0 < \mu < |\nu_{\text{eff}}(q_c, p_c)|$, where

$$\nu_{\text{eff}}(q,p) = \nu + iqv - dq^2 - sp^2 - igqp^2 + hp^4. \tag{48}$$

The frequency on the Hopf bifurcation surface is given by $\omega = \sqrt{|\nu_{\text{eff}}|^2 - \mu^2}$. Recall that this frequency is the difference between half the driving frequency (for $n = 2$) and the frequency of the critical mode. Note that the frequency ω decreases as μ increases, until it goes to zero for $\mu^2 = \mu_0^2(q,p) \equiv |\nu_{\text{eff}}|^2$. At such points, the

Hopf bifurcation is replaced by a steady bifurcation of the trivial solution of the amplitude equations (45). This steady bifurcation leads to (standing) waves which are phase locked to the forcing.

To get some insight into the nonlinear solutions of (45) we consider two limiting cases. Since the phase-locked waves arise through a bifurcation involving a real eigenvalue, the coupled complex equations (45) can be reduced to a single equation sufficiently close to the neutral surface [17]. Depending on the kind of extremum (q_c, p_c) chosen as expansion point, different equations are obtained. Here we concentrate on a situation that eventually leads to an equation of the same form as for the steady bifurcation at a Lifshitz point [25]. Another limiting case is obtained by considering oblique waves within (45), i.e., assuming $|p| > 0$ for small ν and μ. This allows us to derive the amplitude equations (4) from the Lifshitz equations.

We first describe the reduction to a single real Lifshitz equation. The condition for a Lifshitz point for the standing waves on the normal-roll branch is

$$\partial_p^2 \mu^2(q_c, p_c = 0) = 0, \tag{49}$$

where q_c is determined by $\partial_q \mu^2(q_c, p_c = 0) = 0$. These two conditions determine the critical wave number $q = q_c$ and the Lifshitz point in parameter space $s_r = s_r^{\mathrm{LP}}$, respectively:

$$-2(\nu_r - d_r q_c^2) d_r q_c + (v q_c + \nu_i - d_i q_c^2)(v - 2 d_i q_c) = 0, \tag{50}$$

$$s_r^{\mathrm{LP}} = \frac{(\nu_i + v q_c - d_i q_c^2)(s_i + g_r q_c) + g_i q_c (d_r q_c^2 - \nu_r)}{d_r q_c^2 - \nu_r}. \tag{51}$$

Note that the presence of the forcing has shifted the Lifshitz point for the standing waves to a nonzero value of s_r. This is in contrast to the unforced case where the Lifshitz point occurs at $s_r = 0$ with $q_c = p_c = 0$. For large values of v and s_i, of order ϵ^{-2}, this leads to

$$q_c = -\frac{\nu_i}{v}\left(1 + \frac{2\nu_r d_r - \nu_i d_i}{v^2}\right) + \mathcal{O}(\epsilon^8) \tag{52}$$

and a shift of the Lifshitz point to

$$s_r^{\mathrm{LP}} = -\frac{1}{v}\left(\nu_i g_i - 2 d_r \frac{\nu_i s_i}{v}\right) + \mathcal{O}(\epsilon^6). \tag{53}$$

Thus, in this limit of large group velocity v in (45), the steady state neutral surface $\mu^2 = \mu_0^2$ has only a single minimum with $p = 0$; this occurs at $\mu^2 = \mu_c^2 \equiv \mu_0^2(q_c, p_c = 0)$, where q_c is given by (52). (In the special case that v is not large, this need not be the case, as will be discussed below.)

To derive the reduced Lifshitz equation from Eq. (45), we introduce superslow space and time scales and expand μ about its critical value $\mu_c = |\nu_{\mathrm{eff}}(q_c, p = 0, s_r^{\mathrm{LP}})|$, s_r about its critical value s_r^{LP}, while holding ν fixed ($\nu_r < 0$). In particular, we let

$$\mu = \mu_c + \delta^2 \mu_2, \quad s_r = s_r^{\mathrm{LP}} + \delta s_{r1}, \quad X = \delta x, \quad Y = \delta^{1/2} y, \quad T = \delta^2 t, \tag{54}$$

where $0 < \delta \ll 1$. We use the two eigenvectors $(\mu, -\nu_{\mathrm{eff}})^t$ and $(\mu, \nu_{\mathrm{eff}}^*)^t$ of the linear operator evaluated on the neutral surface $\mu^2 = |\nu_{\mathrm{eff}}|^2$, and expand the amplitudes A and B as follows:

$$\begin{pmatrix} A \\ B^* \end{pmatrix} = \delta \begin{pmatrix} \mu \\ -\nu_{\mathrm{eff}} \end{pmatrix} A_1 e^{i q_c x} + \delta^2 \left\{ \begin{pmatrix} \mu \\ -\nu_{\mathrm{eff}} \end{pmatrix} A_2 e^{i q_c x} + \begin{pmatrix} \mu \\ \nu_{\mathrm{eff}}^* \end{pmatrix} B_2 e^{i q_c x} \right\} + \mathcal{O}(\delta^3). \tag{55}$$

At $\mathcal{O}(\delta^2)$ we obtain

$$B_2 = -\frac{1}{2\nu_{\mathrm{eff},r}} \left\{ (v + 2 i q_c d)\partial_X + (s^{\mathrm{LP}} + i q_c g)\partial_Y^2 \right\} A_1, \tag{56}$$

where $\nu_{\mathrm{eff},r} \equiv \mathrm{Re}\{\nu_{\mathrm{eff}}\}$ and ν_{eff} is evaluated at $(q, p) = (q_c, 0)$, and $s^{\mathrm{LP}} \equiv s_r^{\mathrm{LP}} + i s_i$. Projecting the $\mathcal{O}(\delta^3)$ equations onto the left-zero eigenvector $(\mu, -\nu_{\mathrm{eff}})$ the Lifshitz equation,

$$\partial_T A_1 = (\kappa_1 \partial_X^2 + \kappa_2 \partial_Y^2 + i \kappa_3 \partial_X \partial_Y^2 + \kappa_4 \partial_Y^4) A_1 + \Sigma A_1 + \Gamma A_1 |A_1|^2, \tag{57}$$

is obtained, where the coefficients κ_j $(j = 1, ..., 4)$, Σ, and Γ are all real. We find that

$$\Sigma = -\frac{\mu_c \mu_2}{\nu_{\mathrm{eff},r}}, \quad \Gamma = \frac{\mu_c^2}{\nu_{\mathrm{eff},r}} \mathrm{Re}\left\{\nu_{\mathrm{eff}}^* (2\tilde{c} + \tilde{g})\right\}. \tag{58}$$

The coefficients κ_i are given by the appropriate derivatives, with respect to the wave numbers q and p, of the growth rate $\sigma = \nu_{\mathrm{eff},r} + \sqrt{\mu^2 - \nu_{\mathrm{eff},i}^2}$, e.g., $\kappa_1 = \partial_q^2 \sigma(q_c, p_c = 0)$. Note that the direction of bifurcation of the spatially uniform, (nontrivial) steady solution of (57) depends on ν_{eff}, as well as the original nonlinear coefficients $\tilde{c}$ and $\tilde{g}$.

As mentioned before, Eq. (57) has been studied in the case where the bifurcation to the steady uniform solution is supercritical (i.e., in the case where $\Gamma/\Sigma < 0$) [25,28]. These investigations determined that normal and oblique rolls can be stable in two-dimensional wave-number regions, where the shape of these regions depends on the parameter values. In the present context, such solutions correspond to normal phase-locked standing rolls (NPSRo) and oblique phase-locked standing rolls (OPSRo). In the oblique-roll regime stable zigzags arise which connect OPSRo of opposite angles with respect to the director. In addition, undulated solutions can also be stable in small islands in wave-number space [25,28,30]. In the subcritical case, suitable nonlinear gradient terms in X as well as Y direction would have to be included when going to fifth order. They would allow the direction of bifurcation of NPSRo and of OPSRo to differ from each other.

The divergence of B_2 as $\nu_{\text{eff},r} \to 0$ in Eq. (56) shows that the reduced Lifshitz equation (57) is no longer valid in this limit, i.e., as the Hopf bifurcation point is approached. At the Hopf bifurcation and also at the parity-breaking bifurcations from standing structures to traveling structures the full complex Lifshitz equations (45) need to be used. This is not pursued here.

Additional information about possible phase-locked wave patterns is obtained by examining the shape of the neutral surface $\mu^2 = |\nu_{\text{eff}}|^2$ in more detail, where ν_{eff} is given by Eq. (48). For example, an earlier study by Riecke, which pertains to (normal) standing rolls in one spatial dimension, found that the neutral curve need not be convex [17,29]. In fact, it can have two minima, in which case the band of stable wave numbers splits into two disjoint regions, one centered at each of the two minima. This has been investigated, in the one-dimensional case, using the appropriate Ginzburg-Landau equations [17,30], as well as phase equations [17,30,31]. Under the conditions that there are two minima of the neutral curve, it was found that wave-number gradients need not decay as would generally be expected if there was just a single minimum. Instead, stable domain walls can arise which separate regions with different wave numbers q. In the present, two-dimensional study, one may expect that multiple minima with differing values of p can also be obtained in the phase-locked standing-wave regime. We investigate this possibility by examining the form of the neutral surface, associated with the generalized Ginzburg-Landau equations (45), in a special limiting case.

In the one-dimensional case it was shown that for multiple minima of the neutral curve to occur the group velocity must be small [29] [see also Eq. (52)]. Thus to demonstrate the phenomena we choose $v = 0$ as well as $g = 0$. (The minima will then persist for v and g sufficiently close to 0.) Figures 5 and 6 show the neutral surface $\mu^2 = |\nu_{\text{eff}}(q,p)|^2$ for $\nu_r = -0.2$, $d = 1 + i$, $s = -1 + 0.585i$, and $h = -4.27 + 2.5i$ for two different values of ν_i. When $\nu_i = -0.34$ (Fig. 5), there is

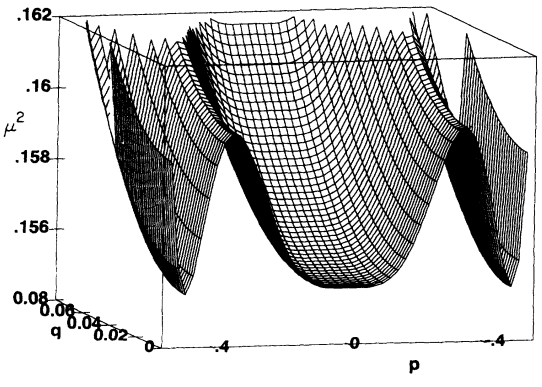

FIG. 5. Neutral surface $\mu^2(q,p)$ for the forced Lifshitz equation (45) with $v = g = 0$, $\nu_r = -0.2$, $d = 1 + i$, $s = -1 + 0.585i$, $h = -4.27 + 2.5i$, and $\nu_i = -0.34$. In the nonlinear regime, zigzag structures are expected to arise. The local wave number of the zigs and of the zags lies in one of the three minima of the neutral surface.

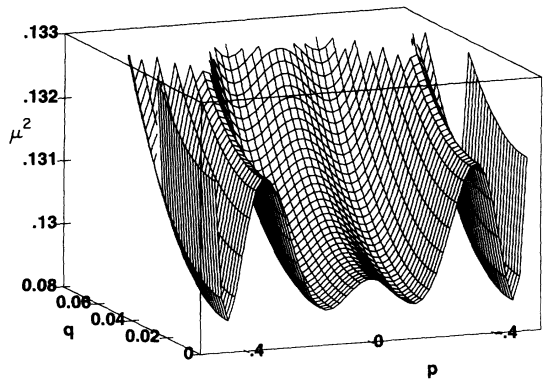

FIG. 6. Neutral surface for $\nu_i = -0.3$. Other parameters as in Fig. 5.

a minimum at $p_c = 0$, $q_c = 0$, corresponding to normal PSRo, as well as a minimum (of roughly the same depth) at $p = \pm p_c \approx 0.45$. Thus in this case one expects a competition between these three kinds of waves which could lead to zigzag patterns consisting of domains with $p = p_c$ and $p = 0$, respectively. In contrast to the zigzags associated with the reduced Lifshitz equation (57) [25], one of the two zigzag directions here is given by the normal direction. Changing the frequency to $\nu_i = -0.3$ shifts the minimum at $p_c = 0$ to a nonzero value (Fig. 6). Now there are four minima and one expects, for example, zigzags consisting of oblique waves with two different positive values of p. In the case that $d_i < 0$, the extremum at $q = 0$ can become a maximum and two new minima (in the q direction) can arise at $q = \pm q_1$. (The reflection symmetry that forces symmetry-related pairs $\pm q_1$, as well as an extremum at $q = 0$, is due to the special choice $v = 0$ and $g = 0$.) Two cases with $d_i < 0$ are shown in Figs. 7 and 8. For $d_i = -0.5$ (Fig. 7) the absolute minima are at $q = 0$ and $p = \pm p_{1,2}$, whereas for $d_i = -0.7$ (Fig. 8) they are at $p = \pm p_1$ and $q = \pm q_1$. Between these two situations the minima of the neutral surface almost degenerate into a circular curve around the local maximum at $q = 0$, $p = \pm 0.35$. (Recall that in the physical system $q = 0$ corresponds to a nonzero wave number $\bar{q}$.) Such a neutral surface, with a minimizing closed curve centered around a finite wave number,

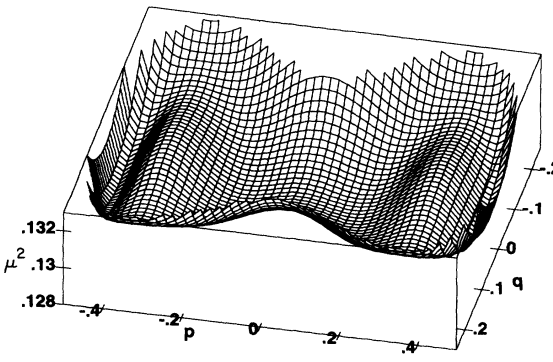

FIG. 7. Neutral surface for $d_i = -0.5$. Other parameters as in Fig. 6.

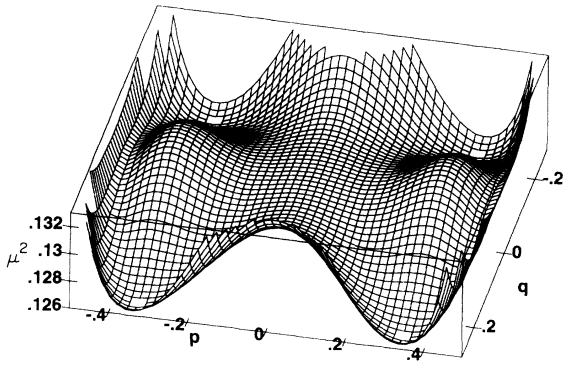

FIG. 8. Neutral surface for $d_i = -0.7$. Other parameters as in Fig. 6.

should lead to interesting nonlinear behavior. Of course, the complicated situations described here are only obtained for special parameter values (e.g., near $v = 0$). Generically, we expect the neutral surface to have only a single minimum. In particular, this is true when the group velocity v in (45) is large.

Finally, we examine the possible stability properties of the spatially periodic, phase-locked standing-wave solutions of the Lifshitz equations (45) in the weakly oblique regime. This is accomplished by deriving the amplitude equations (4) from (45) for $p \neq 0$. Inserting the expansion

$$A = z_1(t)e^{i(qx+py)} + z_4(t)e^{i(qx-py)} + \text{h.o.t.},$$
$$B = z_3(t)e^{-i(qx+py)} + z_2(t)e^{-i(qx-py)} + \text{h.o.t.} \tag{59}$$

into (45), we find that the nonlinear coefficients in (4) in terms of those in (45) are

$$a = \tilde{c},\ b = c = f = \tilde{c} + \tilde{g},\ d = 2\tilde{c}, \tag{60}$$

with ν in (4) replaced by ν_{eff}. It then follows from our stability calculations in Secs. III and IV that PSRe are always *unstable* at onset in the weakly oblique regime. Moreover, PSRo are a stable solution at onset provided $\nu_{\text{eff},r} < 0$ and

$$\text{Re}\{\nu^*_{\text{eff}}(2\tilde{c} + \tilde{g})\} > 0. \tag{61}$$

This is precisely the condition that the PSRo bifurcate supercritically from the trivial solution [cf. Eq. (8)]. That PSRe bifurcate unstably close to the Lifshitz point is consistent with the observation that rectangles are an unstable solution of the reduced Lifshitz equation (57) [25], and that SRe are an unstable solution of the full Lifshitz equations (45) in the absence of forcing ($\mu = 0$) [8].

VI. COMPARISON WITH EXPERIMENTS IN ELECTROCONVECTION

Before comparing our results with the experiments in electroconvection of nematics, it is useful to discuss some of the properties of the unforced experimental liquid-crystal system that are reported in [6]. Without temporal forcing the first instability of the basic state leads to a *steady* roll pattern. Detailed investigation shows, however, strong fluctuations below threshold which are possibly due to thermal noise. Crucial in the present context is the fact that the fluctuations have the character of (oblique) traveling waves. A natural bifurcation diagram which is consistent with these findings is shown in Fig. 9; similar to convection in binary mixtures, there could be a subcritical Hopf bifurcation which leads to unstable waves which in turn merge with a branch of steady rolls. In this bifurcation scenario there is a discontinuous transition from the motionless state directly to finite-amplitude steady rolls when the control parameter is increased beyond the Hopf bifurcation.

Motivated by experiments on binary-mixture convection, where the bifurcation to traveling waves is subcritical [5], the effect of resonant periodic forcing on a *weakly subcritical* Hopf bifurcation to one-dimensional traveling waves has been investigated theoretically [3]. In this subcritical case, it was found that forcing can lead to stable PSW that arise in a supercritical bifurcation already below any saddle-node bifurcation of the unforced (as well as of the forced) branch of traveling waves. In particular, bifurcation diagrams of the kind sketched in Fig. 10, in which the parity-breaking bifurcation of the PSW to TW is subcritical, are possible. If the unforced traveling waves are unstable to a large-amplitude steady structure it is quite natural to assume that this instability persists in the case of sufficiently weak forcing. Thus, at the parity-breaking bifurcation to traveling waves, the system could jump from the PSW to the steady structure as indicated in Fig. 10.

Without temporal forcing the experimental system has two control parameters: the amplitude V and frequency Ω of the applied ac voltage. The bifurcation parameter ν_r depends linearly on the amplitude V, i.e., $\nu_r \propto (V - V_c)/V_c$. The frequency Ω is much greater than the Hopf frequency in the EHC experiments; our amplitude equations apply to the averaged system. The nonlinear coefficients in the amplitude equations (4) depend on Ω and thus can be varied somewhat. The resonant temporal forcing introduces two additional control parameters: the forcing (modulation) amplitude ΔV, or equivalently $|\mu|^n \propto \Delta V^2$, and the detuning $\nu_i = \omega_0 - \omega_e/n$ $(n = 1, 2)$.

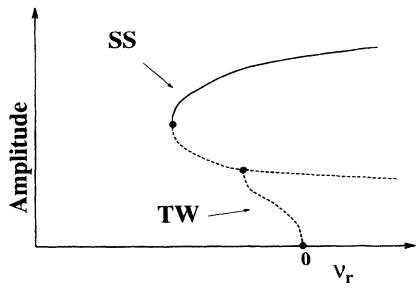

FIG. 9. Sketch of the bifurcation diagram suggested by experiments on electroconvection in nematic liquid crystals.

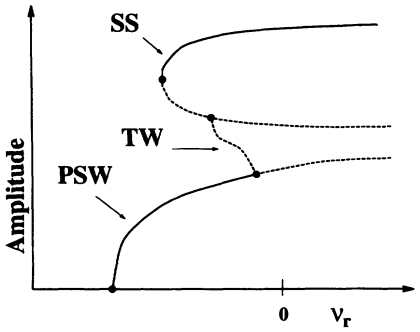

FIG. 10. Effect of a periodic forcing on the subcritical Hopf bifurcation to traveling waves sketched in Fig. 9. The parity-breaking bifurcation of the PSW to TW can be subcritical, thus inducing a jump transition to the steady structure.

In the experiments, four regimes have been identified in the (ν_r, μ) plane, as indicated in Fig. 11. For small applied voltage V (above the open circles) incoherent traveling-wave patches are observed. They are interpreted as driven by noise, which is possibly of thermal origin [22]. This is substantiated by recent measurements of the spatial Fourier spectra [32]. Thus the open circles do not represent a true transition but indicate instead the location where the instrumental sensitivity is sufficient for the detection of very weak fluctuations. When the forcing amplitude is increased, a transition to phase-locked standing waves is found (solid triangles). Depending on the driving frequency Ω they are either standing oblique rolls or standing rectangles and can naturally be identified with the PSRo and PSRe, respectively. When increasing the applied voltage (i.e., ν_r) further, the PSRe lose stability to a structure (at the open diamonds) which is also phase locked to the forcing but is more complicated. During the phase in which the voltage rises the structure is predominantly a "zig". Then the "zag" component increases in strength, leading to a structure which resembles rectangles during the peak of the voltage, whereas the "zag" component dominates during the decay phase. It is reported that this structure—in contrast to the PSRo and PSRe—shows no strong spatial coherence. We interpret this structure as the PSCR bifurcating off the PSRe. Recall that the PSCR is given by $z_1 = z_3 = \mathrm{Re}^{i\Phi}$, $z_2 = z_4 = re^{i\phi}$, so that a typical quantity like the vertical velocity V_z is given by [cf. (1)]

$$V_z = 4R\cos(\omega_e t/n + \Phi)\cos(qx + py) + 4r\cos(\omega_e t/n + \phi)\cos(qx - py) + \text{h.o.t.} \quad (62)$$

Thus, provided $\Phi - \phi$ is not a multiple of π, the two standing waves differ in their phase with respect to the forcing; the structure alternates between "zigs" [for values of t such that $\cos(\omega_e t/n + \phi) = 0$], "zags" [when $\cos(\omega_e t/n + \Phi) = 0$], and rectangles [when $|R\cos(\omega_e t/n + \Phi)| = |r\cos(\omega_e t/n + \phi)|$]. Figure 12 shows a representative sequence of PSCR structures. Since the two amplitudes r and R are different, there exist two symmetry-related PSCR solutions, one in which the "zigs" dominate $(R > r)$ and one in which the "zags" dominate $(r > R)$. When the PSRe solution loses stability to PSCR, both zig- and zag-dominated PSCR are expected to arise and compete with each other, with domains separated by grain boundaries forming. It is tempting to attribute the spatial incoherence observed in the experiments to the existence of such domains. Unfortunately, the reported experiments do not provide enough data to investigate this interesting question.

When the applied voltage is increased further a transition to a steady structure occurs (to the right of the solid squares) which is modulated in its amplitude. This transition is beyond the scope of the present analysis. One may speculate that it is related to the fact that the initial Hopf bifurcation seems to be weakly subcritical (cf. Fig. 9): without temporal forcing the system jumps directly to a steady branch. In the presence of forcing this could render the parity-breaking bifurcation of the PSRe subcritical. The system would then jump from the PSCR directly to the steady branch as indicated in Fig. 10. We have not studied the stability of the PSCR. Since the instability of the PSRe to TRe leads out of the

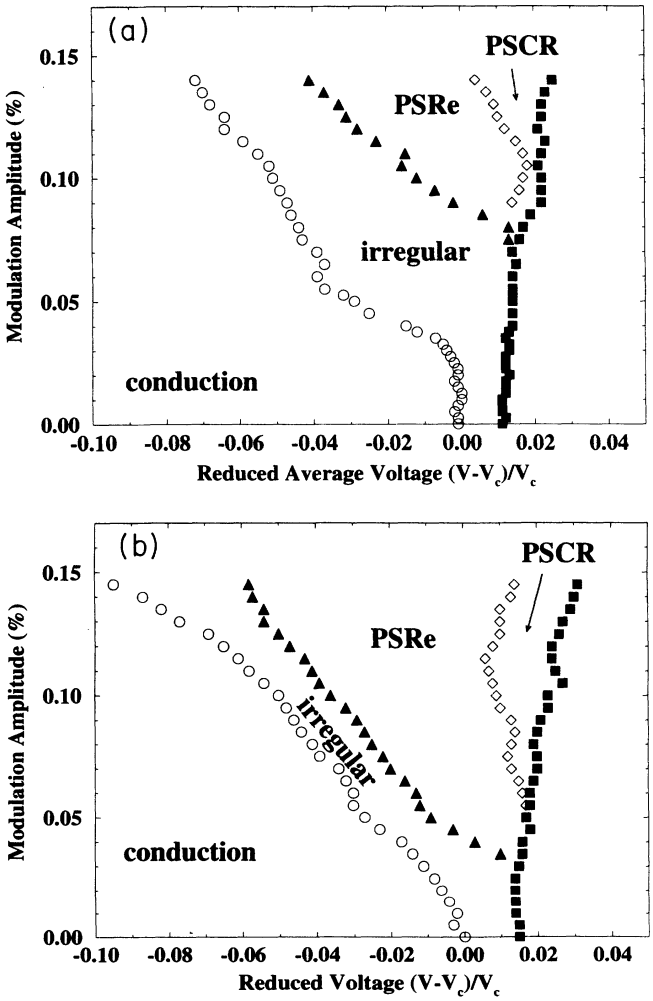

FIG. 11. Experimental phase diagram for temporally forced convection in nematic liquid crystals, reproduced from [6]. (See the text for a discussion of the various regions.) (a) $\Omega = 0.50$ Hz, (b) $\Omega = 0.31$ Hz.

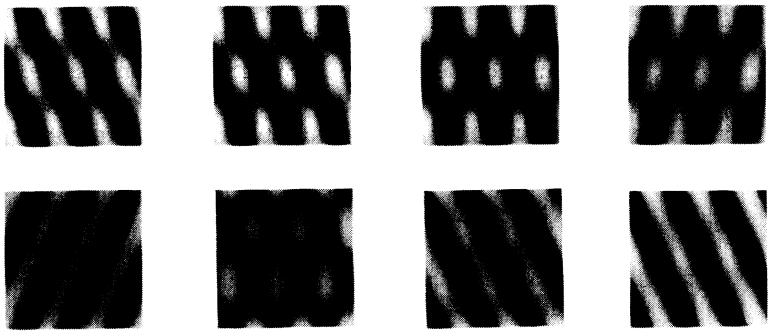

FIG. 12. Typical time sequence for a representative phase-locked standing-cross-rolls solution (PSCR). Note that the structure alternates between a zig- and a zag-dominated state.

standing-wave subspace, which also contains the PSCR, one might expect that they inherit that instability, and consequently, also exhibit a jump transition to the steady structure.

The present analysis suggests that the parameter ρ, which governs the competition between the different standing structures, can be made small by choosing a suitable detuning ν_i [cf. (16)]. If this could be achieved below the unforced Hopf bifurcation ($\nu_r < 0$), both transitions from PSCR to PSRo and to PSRe could be observed at small amplitudes below the onset of the Hopf bifurcation in the unforced case. In the experimental system the wave number of the structure is, however, not fixed. Instead, the system can choose a wave number from a continuum of values within the stability limits. In particular, if $\mathbf{v} = v_x\hat{x} + v_y\hat{y}$ is the group velocity in the oblique regime, then a change $\Delta q\hat{x} + \Delta p\hat{y}$ in the wave vector shifts the detuning to an effective value: $\nu_{\text{eff},i} = \nu_i + v_x\Delta q + v_y\Delta p + \mathcal{O}(\Delta q^2, \Delta p^2, \Delta q\Delta p)$. Similarly, near the Lifshitz point, the effective detuning at the critical wave number $(q_c, p_c = 0)$, with q_c given by (52), is strongly reduced and can remain small over a range of frequencies; in particular, $\nu_{\text{eff},i} = \nu_i + vq_c - d_i q_c^2 = \mathcal{O}(\epsilon^4)$ [17]. This may explain why in the experiments the location of the transition to PSCR, which depends on the detuning ν_i or more precisely $\nu_{\text{eff},i}$, did not change substantially even though the forcing frequency was changed by almost 50%.

Finally, our analysis suggests that a transition to PSCR may also be found if the frequency Ω is chosen such that the first transition is not to rectangles but to standing oblique rolls (PSRo), as long as ρ is positive and not too large in the regime where the PSRo arise. Experimentally this has not been tested in detail.

VII. CONCLUSION

In summary, we have studied the effect of a resonant temporal forcing on oblique traveling waves close to onset in an anisotropic system. We have found that such a forcing can excite various standing-wave structures which are phase locked to the forcing: rolls, rectangles, and cross rolls. The latter arise in secondary bifurcations from either the phase-locked roll or rectangle structures, and in many cases (if not all) provide a transition between them. These bifurcations depend strongly on external control parameters such as the forcing frequency (effective detuning). In particular, if the wave number of the structure could be fixed, one would be able to choose the control parameters such that a wide variety of bifurcation scenarios could be observed. In the general case, however, the attainable effective detuning is limited. Nevertheless, by adjusting the frequency Ω of the applied ac voltage in the unforced case, so that the system is close to a transition between standing rolls and rectangles, the available detuning may be sufficient to observe the transition from phase-locked standing rolls to phase-locked standing rectangles via the general cross-rolls solution.

A striking feature of the standing rolls and rectangles observed in the experiments is their strong spatial coherence. This is perhaps not surprising since they arise through bifurcations in the amplitude equations that involve only real eigenvalues. Close to onset, the standing rolls can be modeled by a single Ginzburg-Landau equation with real coefficients. This equation admits a stable band of wave numbers and exhibits diffusive phase dynamics; moreover, it can be derived from a potential. Similarly, we expect the standing rectangles to be described by two coupled Ginzburg-Landau equations with real coefficients. We propose that the spatial incoherence associated with the standing cross rolls may be due to the formation of grain boundaries separating domains of symmetry-related structures. A more detailed experimental, as well as theoretical, investigation of this regime would be interesting. Such studies could reveal whether this interpretation is correct and, if so, identify the dynamics associated with the domain walls.

In the vicinity of a Lifshitz point, we model the system by two coupled complex generalized Ginzburg-Landau equations which take into account the spatial degrees of freedom. We find, in this regime, that the phase-locked standing rectangles are always unstable. Phase-locked standing rolls are the preferred spatially periodic solution in this regime.

Finally, the results presented in this paper may also be pertinent to parametrically forced systems which do not exhibit a Hopf bifurcation, but which do support weakly damped waves. This, for instance, is the case in the Faraday experiment for low-viscosity fluids.

ACKNOWLEDGMENTS

We would like to thank M. de la Torre Juárez and I. Rehberg for discussing their experiments with us, and E. Knobloch for useful discussions on subjects related to

this paper. This work was supported by NATO collaborative research Grant No. 900276. H.R. acknowledges support from the NSF/AFOSR under Grant No. DMS-9020289 and support by DOE Grant No. DE-FG02-92ER14303. M.S. and H.R. would like to thank the University of Bayreuth, where much of this work was done, for its hospitality. Part of this work was also carried out at the Institute for Theoretical Physics at the University of California, Santa Barbara, which is supported by NSF Grant No. PHY89-04035.

[1] H. Riecke, J.D. Crawford, and E. Knobloch, Phys. Rev. Lett. **61**, 1942 (1988).
[2] D. Walgraef, Europhys. Lett. **7**, 495 (1988).
[3] H. Riecke, J.D. Crawford, and E. Knobloch, in *The Geometry of Nonequilibrium,* edited by P. Coullet and P. Huerre (Plenum Press, New York, 1991), p. 61.
[4] C.D. Andereck and J.J. Hegseth (private communication).
[5] I. Rehberg, S. Rasenat, J. Fineberg, M. de la Torre Juárez, and V. Steinberg, Phys. Rev. Lett. **61**, 2449 (1988).
[6] M. de la Torre Juárez and I. Rehberg, Phys. Rev. A **42**, 2096 (1990).
[7] M. Silber and E. Knobloch, Nonlinearity **4**, 1063 (1991).
[8] M. Silber, H. Riecke, and L. Kramer, Physica D **61**, 260 (1992).
[9] W. Zimmermann, in *Defects, Singularities and Patterns in Nematic Liquid Crystals: Mathematical and Physical Aspects*, Vol. 332 of *NATO Advanced Study Institute, Series C*, edited by J.M. Coron, J.M. Ghidaglia, and F. Hélein (Kluwer, Dordrecht, 1991), p. 401.
[10] E.g., A.B. Ezerskii, M.I. Rabinovich, V.P. Reutov, and I.M. Starobinets, Sov. Phys. JETP **64**, 1228 (1986); S. Douady, S. Fauve, and O. Thual, Europhys. Lett. **10**, 309 (1989).
[11] H. Suhl and X.Y. Zhang, Phys. Rev. Lett. **57**, 1480 (1986).
[12] See, for example, J. Guckenheimer and P. Holmes, *Nonlinear Oscillations, Dynamical Systems, and Bifurcations of Vector Fields* (Springer, New York, 1986), and references therein.
[13] L. Kramer, E. Bodenschatz, W. Pesch, W. Thom, and W. Zimmermann, Liq. Cryst. **5**, 699 (1989).
[14] I. Rehberg, S. Rasenat, and V. Steinberg, Phys. Rev. Lett. **62**, 756 (1989).
[15] By using fluids with high viscosity not only square patterns but also roll patterns can be obtained [S. Fauve (private communication)]. To what extent the present approach is adequate in this regime is not clear, since it assumes weak damping, i.e., small viscosity.
[16] G. Dangelmayr and E. Knobloch, Philos. Trans. R. Soc. London, Ser. A **322**, 243 (1987).
[17] H. Riecke, Europhys. Lett. **11**, 213 (1990).
[18] E.g., in M. Golubitsky, I. Stewart, and D.G. Schaeffer, *Singularities and Groups in Bifurcation Theory, Vol. II* (Springer, New York, 1988).
[19] M. Golubitsky and M. Roberts, J. Differ. Equ. **69**, 216 (1987).
[20] J.D. Crawford and E. Knobloch, Physica D **31**, 1 (1988).
[21] C. Elphick, E. Tirapegui, M.E. Brachet, P. Coullet, and G. Iooss, Physica D **29**, 95 (1987).
[22] I. Rehberg, S. Rasenat, M. de la Torre Juárez, W. Schöpf, F. Hörner, G. Ahlers, and H.R. Brand, Phys. Rev. Lett. **67**, 596 (1991).
[23] W. Zimmermann and L. Kramer, Phys. Rev. Lett. **55**, 402 (1985).
[24] I. Rehberg, B.L. Winkler, M. de la Torre Juárez, S. Rasenat, and W. Schöpf, *Festkörperprobleme/Advances in Solid State Physics*, edited by U. Rössler (Vieweg, Braunschweig, 1989), Vol. 29, p. 35.
[25] W. Pesch and L. Kramer, Z. Phys. B **63**, 121 (1986).
[26] E. Knobloch and J. De Luca, Nonlinearity **3**, 975 (1990); E. Knobloch, in *Pattern Formation in Complex Dissipative Systems*, edited by S. Kai (World Scientific, Singapore, 1992).
[27] B.J. Matkowsky and V. Volpert, Physica D **54**, 203 (1992).
[28] E. Bodenschatz, M. Kaiser, L. Kramer, W. Pesch, A. Weber, and W. Zimmermann, in *The Geometry of Non-Equilibrium,* edited by P. Coullet and P. Huerre (Plenum Press, New York, 1991), p. 111.
[29] H. Riecke, in *Nonlinear Evolution of Spatio-Temporal Structures in Dissipative Continuous Systems,* edited by F.H. Busse and L. Kramer (Plenum Press, New York, 1990), p. 437.
[30] D. Raitt and H. Riecke, in *Spatio-Temporal Patterns in Nonequilibrium Complex Systems,* edited by P.E. Cladis and P. Palffy-Muhoray (Addison-Wesley, Reading, MA, in press); D. Raitt and H. Riecke (unpublished).
[31] H.R. Brand and R.J. Deissler, Phys. Rev. Lett. **63**, 508 (1989).
[32] B. Winkler, Ph.D. thesis, Universität Bayreuth, 1993 (unpublished).

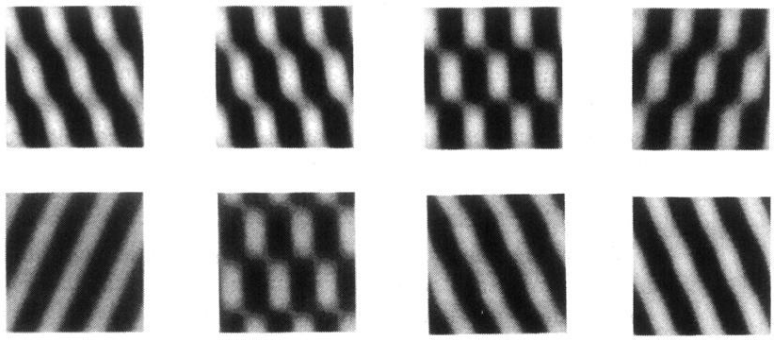

FIG. 12. Typical time sequence for a representative phase-locked standing-cross-rolls solution (PSCR). Note that the structure alternates between a zig- and a zag-dominated state.